J Mater Sci (2024) 59:6048–6058

Uniform strain high-pressure torsion (US-HPT): an approach to reduce strain gradients

A. Hohenwarter[1,*], and S. Wurster[2]

[1] *Chair of Materials Physics, Department of Materials Science, Montanuniversität Leoben, Jahnstraße 12, 8700 Leoben, Austria*
[2] *Erich Schmid Institute of Materials Science, Austrian Academy of Sciences, Jahnstraße 12, 8700 Leoben, Austria*

Received: 29 September 2023
Accepted: 10 November 2023
Published online: 3 December 2023

ABSTRACT

Based on the pioneering work of Erbel, we propose a simple modification of classical high-pressure torsion anvils that allows a strong reduction or even elimination of the inherent strain gradient in disk-shaped samples deformed by high-pressure torsion. This is realized by using an adapted anvil design, which entails a linearly varying depth of the anvil's depression with the radius. In order to compare results of using the modified anvil design with classical flat anvils, a comparative study using high purity nickel was performed. The possible change in the strain gradient is assessed with hardness and microstructural investigations. The results prove that the strain gradient can be considerably reduced or even eliminated. The technical features of this technique, in the following termed as uniform strain high-pressure torsion (US-HPT), are presented with this feasibility study and practical limitations are discussed.

Handling Editor: Megumi Kawasaki.

Address correspondence to E-mail: anton.hohenwarter@unileoben.ac.at

https://doi.org/10.1007/s10853-023-09147-2

GRAPHICAL ABSTRACT

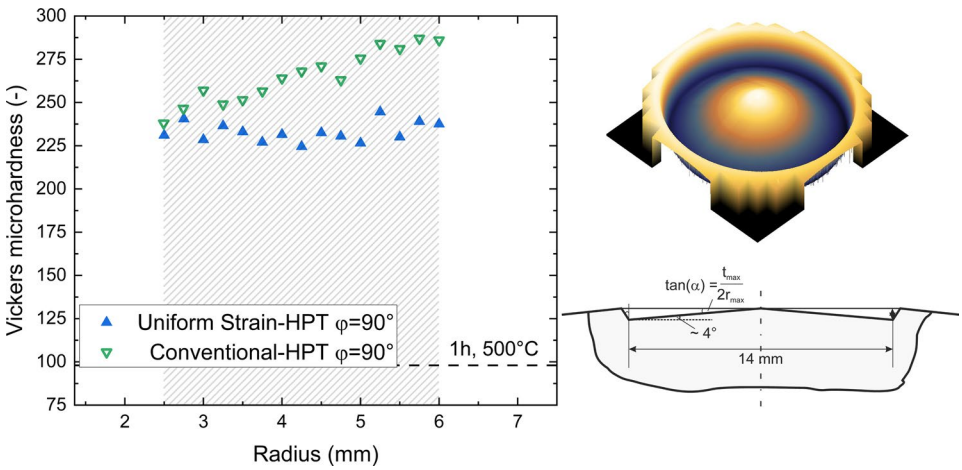

Introduction

The use of high-pressure torsion (HPT) for material synthesis in the field of severe plastic deformation has become a widespread technique in the community that can be understood by numerous advantages of this technique: (i) the technical simplicity of the process; (ii) well controllable parameters such as introduced shear, process temperature and shear strain rate; (iii) applicability of HPT to high strength and difficult to deform materials; and (iv) high versatility in material selection including the usage of powders as starting materials, but also the deformation of composites, ceramics and semiconductors [1–4].

It is evident that the strain or any other definition of an equivalent strain of classical HPT will scale with the radius [5]. The radius dependency is often promoted as an advantageous feature as within one sample, the evolution of microstructure and mechanical properties such as hardness can be investigated very efficiently over a wide range of structural changes, especially as long as the strain gradient within the sample remains small. In addition, due to the natural deceleration of the microstructural changes with increasing strain, which is often interpreted as a saturation behavior [2], a homogenization of the microstructure and mechanical properties over large areas of the processed disks is enabled.

Despite these beneficial process features, the strain gradient can also lead to experimental problems when intermediate deformation states are desired. For example, it is known that besides grain refinement, the misorientation distribution and thus the ratio of low- to high-angle boundaries changes upon deformation [2]. A specific misorientation distribution departing from the one in the saturation state might be beneficial for a balanced ratio of strength to ductility or fracture resistance. Measurements on materials processed by equal-channel angular pressing, subjected to considerably lower amounts of strain than typically applied for HPT-processed materials, point into this direction [6]. If such intermediate microstructural states are envisaged for mechanical tests and the specimen volume should be large so that a certain mesoscopic specimen can be extracted, the presence of the gradient in HPT-processed disks potentially leads to an averaging effect over the investigated volume. Therefore, it would be advantageous to reduce or even remove the strain gradient and expand a specific desired microstructural state across large parts of the HPT-processed disk. The same issue of large and unwanted structural variations at low applied strains within one disk may also arise for functional properties and applications, such as for the production of magnetic materials. Weissitsch et al. found an optimum applied shear strain for Fe-$SmCo_5$ composites when screening the magnetic properties as a function of radius [7]. Consequently, once an optimum state is found for a certain applied shear strain, it would be again desirable to obtain this intermediate deformation state in larger volumes, which is impossible for classical HPT.

From the theoretical view point, it may also be interesting to analyze the microstructural evolution in HPT with the absence of a pronounced strain gradient,

for example, considering the role of strain gradient plasticity for grain refinement [8]. Finally, it is well known that residual stresses are present in HPT disks [9] and the reduction of the strain gradient may be helpful to reduce them.

To overcome the limitation of strain gradients being present within HPT-deformed material, we propose here a simple modification of quasi-constrained HPT and pick up the approach of Erbel, who already used a very similar setup almost 45 years ago [10], however did not describe and analyze the local strain gradient or hardness distribution in detail and used the processed samples for analyzing the mechanical properties of extremely strain-hardened copper on the macroscale. By applying an adapted HPT anvil design that we term uniform strain high-pressure torsion (US-HPT), some of the raised points concerning the elimination of strain gradients will be addressed.

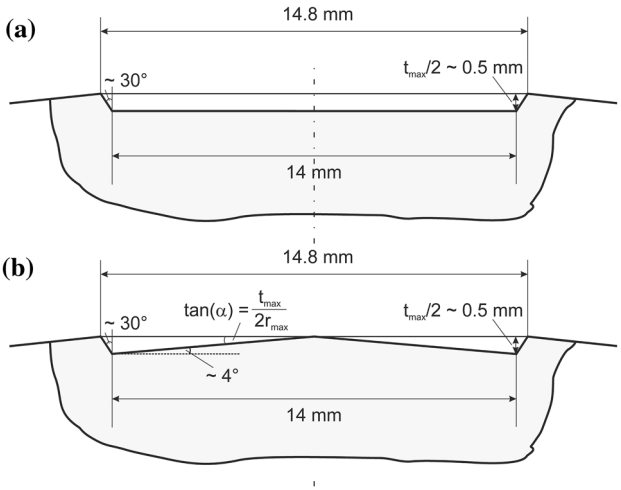

Figure 1 Schematic detail and dimensions of the depressions in the used HPT anvils. **a** Classical anvil design with a flat depression. **b** Cross section of the adapted HPT anvil design for US-HPT having a conical depression.

Material and methods

In the case of quasi-constrained, conventional HPT processing (HPT), using anvils of constant depth, the shear strain γ can be expressed by:

$$\gamma(r) = \frac{2\pi r}{t} \cdot n, \tag{1}$$

where r is the radius, t is the thickness of the sample and n is the number of rotations. A corresponding anvil will have for this sample design a flat depression, as presented in Fig. 1a. Note that for the depth of the depression also the variable t is in use, which has been before introduced as the thickness of the sample. The thickness of the sample and the depth of the depression multiplied by two are equivalent when the elastic distortion of the anvils and the thickness of the outflowing material are neglected. Usually, the elastic distortion and the finite thickness of the rim lead to a somewhat thicker sample.

In this study, rather small strain increments are applied; therefore, it is more useful to substitute n in Eq. 1 with $n = \phi/360°$, where ϕ is the applied rotational angle in terms of degrees. Even though t will slightly change during deformation as material is extruded between the anvils' rim, it can be regarded as constant after the imposition of large strains. The same assumption can be made for samples that have been pre-shaped to a thickness very close to the depth of the anvils. For samples of constant thickness t, the strain will vary linearly with the radius. In order to obtain a constant strain, the thickness of the sample must linearly vary with the radius as shown in Fig. 1b, where the adapted anvil design for this study is presented.

Here, t is a linear function of r and can be written as $t = 2 \cdot \tan(\alpha) \cdot r$. The theoretical imposed shear strain can be now written as:

$$\gamma = \frac{\pi}{\tan\alpha} \cdot \frac{\varphi}{360°} = \frac{\pi n}{\tan(\alpha)} \tag{2}$$

The shear strain will only depend on the number of rotations, i.e., the applied rotational angle, respectively. In addition, the strain increase can be adjusted by changing the angle α, but for doing so a different pair of anvils is needed. The angle α, which is in the present work about 4°, characterizes the change of the local specimen thickness or, in other words, the taper of the depression. In order to investigate to which extent this idea can be realized in an experiment, a feasibility study comparing both anvil designs (Fig. 1) was conducted.

As a well-researched and simple model material pure nickel (purity: 99.99 wt%, purchased from Goodfellow) was selected [11]. From Fig. 1b, it is evident that the adapted anvil design will also lead to a certain strain gradient for small radii (small local sample thickness), induced by the compressive deformation before HPT deformation when samples

with a uniform thickness are used as a starting sample. Therefore, to study precisely the effect of the modified anvil design on the strain distribution, all samples (HPT and US-HPT) were pre-deformed up to 2 full rotations in the respective anvil design and afterward annealed at 500 °C in atmosphere before the actual shear deformation experiment (either HPT or US-HPT) was performed. With this procedure, it was attempted to keep the plastic deformation induced by the compressive deformation in the subsequent experiment to a minimum. The combination of deformation and heat treatment led to an initial grain size in the range of a couple hundred of micrometers.

For the comparison of samples processed by HPT and US-HPT, following samples were processed: using HPT one sample after the aforementioned preconditioning (2 rotations plus annealing) was deformed to a rotational angle of 90°. An angle of 90° is equivalent to a maximum shear strain of 8.2 at the outer radius of 7 mm, considering a final measured thickness of 1.34 mm. The sample before deformation was about 1.66 mm. The induced compressive deformation was therefore small and in the range of 20% so that the compressive deformation can be neglected in comparison to the large strain applied by torsion. This reference deformation state was chosen as earlier studies showed that the applied shear strain will lead to a pronounced gradient in the hardness of the sample [2]. Preconditioned samples, using US-HPT, were deformed up to 30°, 60° and 90°, which results in a nominal constant shear strain of 3.7, 7.3 and 11.0, respectively, taking into account Eq. (2), and the final sample thickness of 1 mm at $r = 7$ mm. The sample before deformation was about 1.03 mm so that the compressive deformation can be generally neglected. All experiments were carried out at the same constant nominal pressure of 2.3 GPa (referred to a maximum diameter 14.8 mm, (see Fig. 1) at ambient temperature with a rotational speed of 0.2 rotations/minute.

The strain gradient was indirectly sampled by measuring the hardness distribution within the HPT and US-HPT disks with a microhardness tester (DuraScan, Zwick Roell) equipped with a Vickers indenter using a load of 200 gf. Indents were made on cross sections of the deformed disks along the radius from the center ($r = 0$ mm) to the edge ($r = 7$ mm). The very edge of all disks as well as the very center of US-HPT samples were excluded from the analysis due to the complicated deformation state as will be discussed later. In addition, comprehensive microstructural investigations were carried out using a Tescan Magna scanning electron microscope equipped with an electron backscatter diffraction (EBSD) system of Bruker (e$^-$Flash^{FS}). EBSD data were analyzed using Bruker Esprit (version 2.3) and OIM data analysis (version 5.31), and for all investigations, a step-size between 50 and 200 nm was used depending on the field of view.

Results

Figures 2 and 3 present the microstructural evolution of both principal types of deformed samples, HPT and US-HPT. The microstructure is substantially changing for the HPT sample along the radius from the coarse-grained recrystallized state to a severely deformed ultrafine state, compare Fig. 2a, d. For better comparison, the field of view was kept constant for all images. Figure 2a shows the interior of one single grain with small fluctuations of the local orientation, which is an effect of a slight deformation during the initial compression step. For larger radii, i.e., higher strains, typical microstructural changes become evident, such as larger fluctuations of orientations within single grains (Fig. 2b), cell formation (Fig. 2c) and the evolution of a high density of high-angle grain boundaries (HAGBs), see Fig. 2d. The described changes in the microstructure coincide well with former studies performed on pure Ni [12–14]. When the same microstructural analysis for the US-HPT sample, deformed to the same rotation angle, is performed, the situation is markedly different. The microstructural appearance is rather constant, see Fig. 3.

For a quantification of this qualitative observation, the grain average misorientation (GAM) distribution and the normalized density of low-angle grain boundaries (LAGBs, $> 2°$ and $< 15°$ misorientation) and HAGBs ($> 15°$ misorientation) are presented in Fig. 4 and Fig. 5. For the HPT sample, there is a large difference in normalized LAGB density along the radius. In Fig. 4, it can be seen that the LAGB density has its maximum for medium radii, while the HAGB density continues to increase. Further microstructural refinement and increased hardness can be expected for samples deformed to higher rotation angles. For the US-HPT sample, both grain boundary densities start at a higher level ($r = 2$ mm), but densities decrease and level off at larger radii. Both findings, the appearance of a slightly stronger deformed microstructure

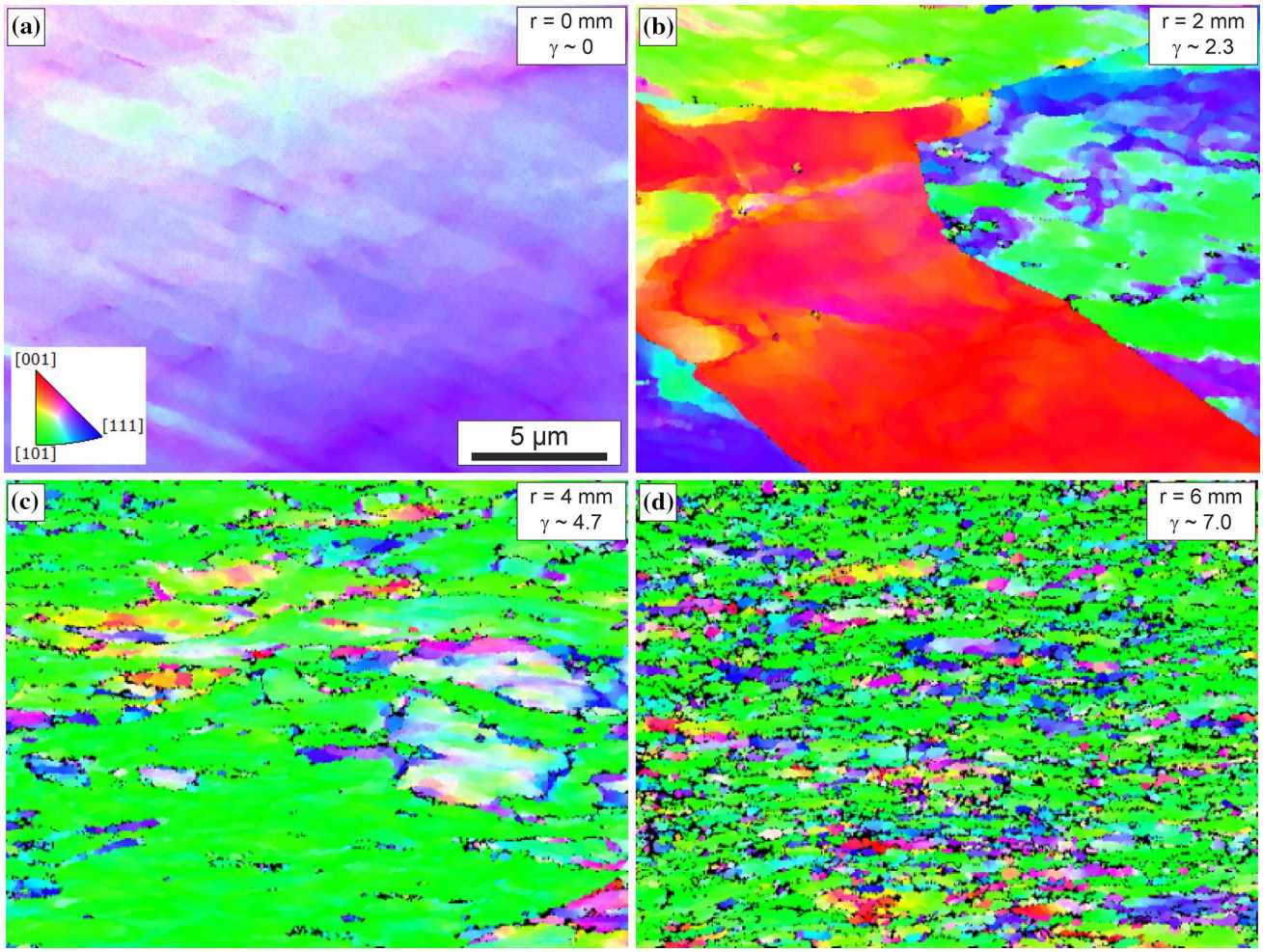

Figure 2 IPF maps recorded in tangential direction at different radii of the HPT sample deformed to a rotational angle of 90°. **a** $r = 0$ mm ($\gamma \sim 0$), **b** $r = 2$ mm ($\gamma \sim 2.3$), **c** $r = 4$ mm ($\gamma \sim 4.7$) and **d** $r = 6$ mm ($\gamma \sim 7.0$). Scale bar applies to all subfigures.

(Fig. 3a) and a slightly higher grain boundary density for $r = 2$ mm for the US-HPT sample will be discussed later by deviations of the applied strain for small radii.

Beside the possibility of using inverse pole figure (IPF) maps and grain boundary types and length, GAM distributions also serve as a proper method for comparing microstructures subjected to different degrees of deformation (Fig. 5). GAM distributions summarize the misorientation between each pixel of an individual grain and the average orientation of that grain.

For a single crystal, the distribution would peak at very low misorientation angles, which originate from small, but existing orientation changes or from orientation noise in the EBSD data. With increasing number of stored dislocation and evolving dislocation cell structures, the distribution broadens. With increasing refinement of the microstructure and the evolution of a high-density network of HAGBs, fewer dislocations are stored within grains. Misorientations within grains are reduced and the shape of GAM distribution returns to its original single-crystalline shape. For the HPT sample (Fig. 5a), there is a strong change in the GAM distribution and the described process from single-crystalline-like behavior towards broad distributions, returning to a sharp distribution can be found. In contrast to the large changes in the GAM distribution for the HPT sample, the US-HPT specimen (Fig. 5b) shows an almost constant GAM distribution for all investigated radii (2–6 mm).

Hardness values of all HPT and US-HPT are summarized in Fig. 6. In addition to the 90°, US-HPT sample also data of US-HPT samples deformed to 30° and 60° are presented to better present the

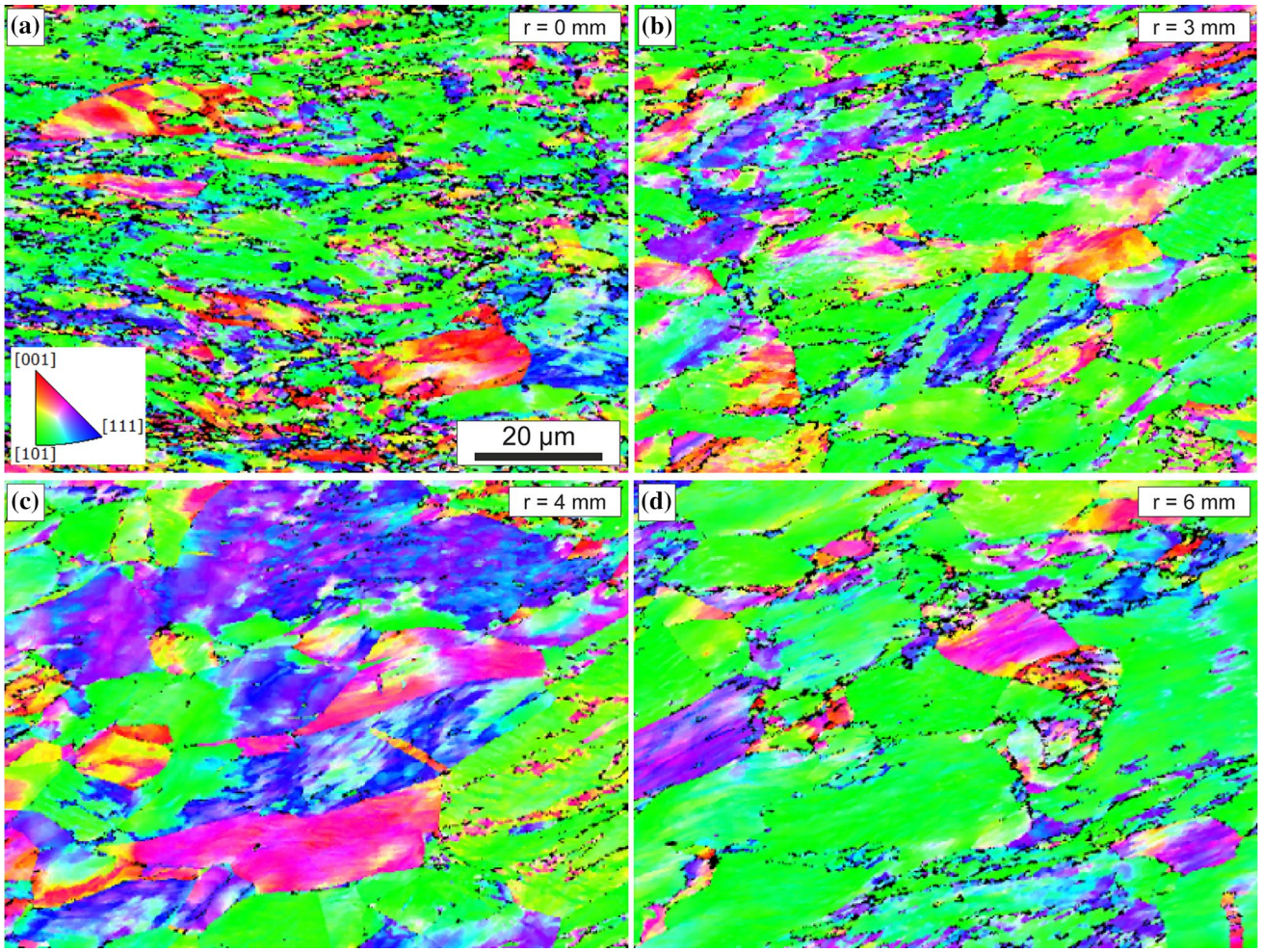

Figure 3 IPF maps recorded in tangential direction at different radii of the US-HPT sample deformed to a rotational angle of 90° ($\gamma_{const} \sim 11$). **a** $r = 2$ mm, **b** $r = 3$ mm, **c** $r = 4$ mm and **d** $r = 6$ mm. Note the different scale bar compared to Fig. 2. Micron bar applies to all subfigures.

hardness evolution for nominal constant shear strains. It is evident that the 30° and 60° samples show a similar hardness range, which indicates that some slippage might have occurred for the 60° sample. The slippage issue is always to consider when rather small pressures, such as in this study, are applied [15, 16]. The HPT sample deformed for 90° shows the as expected increase with increasing radius and increasing applied shear deformation. Constant hardness values were found for the US-HPT samples for regions between radii of 2.5 mm and 6 mm. For smaller and larger radii, deviations from that were observed, which are in the center of the subsequent discussion.

Discussion

As presented in the previous section, results on microstructure and hardness provide evidence that the adapted anvil design has a beneficial effect on the homogeneity of applied shear deformation. However, there are considerable deviations for small and large radii, which require further discussion.

One significant point that needs to be taken into account when analyzing the hardness and microstructural data of US-HPT samples is a possible deviation of the final sample shape from the perfect geometry. Equation 2 presumes a sample thickness of 0 mm for $r = 0$ mm, so to say a perfect tip of the conical shape

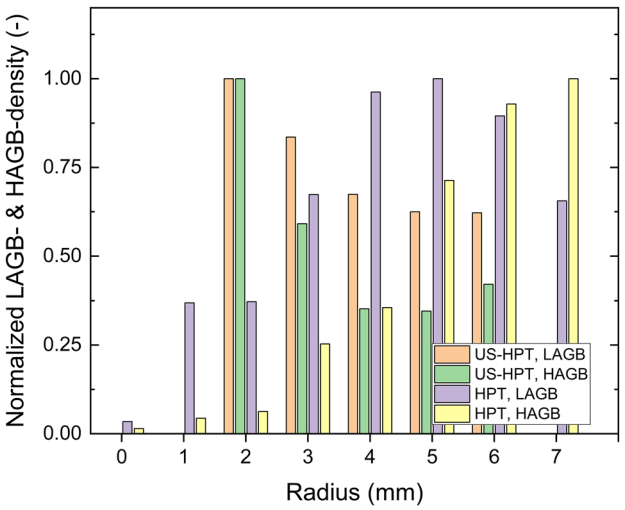

Figure 4 Normalized density of LAGB (2°–15°) and HAGB (> 15°) for US-HPT and conventional HPT at different radii. Note, for conventional HPT, the scan size was adapted to accommodate the strongly varying microstructure. For US-HPT sample, the scan size and step size were constant, 100 µm and 200 nm, respectively, see Fig. 3.

of the depression. However, due to practical reasons and inaccuracies during sample preparation and subsequent deformation, the final sample shape may show a small perforation, when the conical shape of the anvils punctures the sample during deformation. On the other hand, the initial sample could also be too thick at $r = 0$ mm, resulting in a finite thickness t_{min} in the center of the sample even after deformation. Both deviations in sample shape lead to a variation in the resulting calculated shear strain distribution for small radii, whose general trends for different extreme cases are discussed.

In Fig. 7, the strain evolution for different geometries for a maximum sample thickness at $r = 7$ mm of 1 mm after a quarter rotation is exemplarily shown. In a sample having a perfect geometry as described in Eq. 2, the shear strain would be in fact constant. For a conventional HPT sample with a constant and identical thickness at $r = 7$ mm, the strain would increase linearly with the maximum and identical strain at $r = 7$ mm as the perfect US-HPT sample geometry. The two afore-described deviations from the perfect US-HPT processed samples show however pronounced differences in the strain distribution. To calculate these differences as shown in Fig. 7, differing values of thickness, compared to a perfect sample, have to be considered, and Eq. (1) has to be adapted slightly:

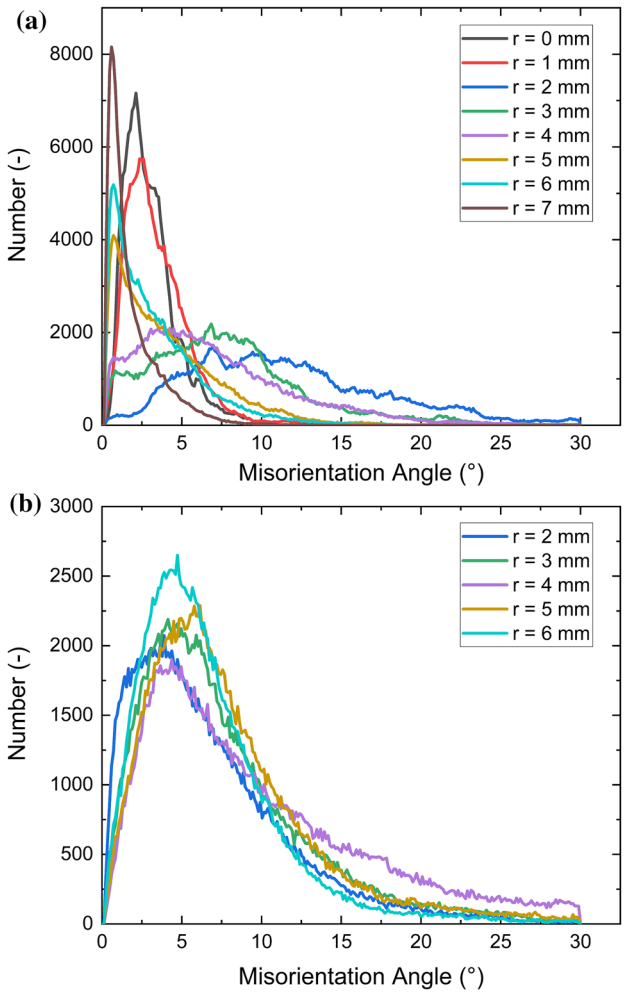

Figure 5 Grain average misorientation distribution for the HPT (**a**) and US-HPT (**b**) specimen, both deformed to 90° rotations. In contrast to HPT, the GAM distribution using US-HPT remains similar.

$$\gamma(r) = \frac{2\pi r}{t(r)} \cdot n, \tag{3}$$

For the two possible cases, a) hole of radius r_{hole} in the center and b) a finite thickness t_{min} at the center, $t(r)$ can be given in the form

$$a)\, t\left(r \le r_{hole}\right) = 0; t\left(r > r_{hole}\right) = 2\tan(\alpha)\left(r - r_{hole}\right) \tag{4.1}$$

$$b)\, t(r) = t_{min} + 2\tan(\alpha) r \tag{4.2}$$

For a sample containing a hole (perforation), a finite value of the sample thickness is only present for radii larger than r_{hole}, which leads to a singular behavior of the strain at r_{hole} with decreasing trend toward large

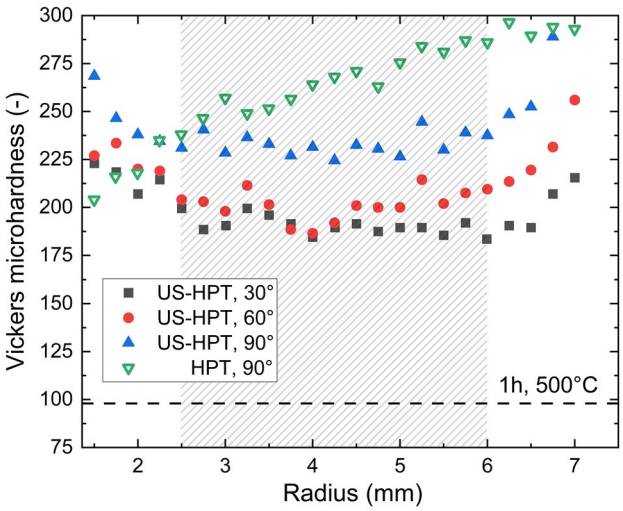

Figure 6 Hardness values of HPT (90° rotation) compared with US-HPT samples (30°, 60° and 90° rotation) which received constant nominal shear strains of 3.7, 7.3 and 11.0, respectively. The classical HPT sample rotated to 90° corresponds to a nominal shear strain of 8.2 at maximum radius. All hardness measurements are shown as a function of sample radius. The initial hardness value after recrystallization for 1 h at 500 °C is also provided. The dashed region shows the part of the US-HPT samples featuring a considerably constant hardness level.

radii and final convergence of the value with the US-HPT and conventional design. In addition, the compressive deformation applied before shear deformation becomes large for small radii of US-HPT samples. In strong contrast, samples that possess a small, but finite thickness t_{min} show a stronger increase of strain for small radii compared to the conventional design, and the strain converges again toward the value of the other sample geometries. Examples of these extremes are presented in Fig. 8. Figure 8a presents a cross section of a sample deformed to 45° stemming from a pre-experiment where a perforation occurred. Due to the large perforation, the specimen was excluded from the study. The second extreme is shown in Fig. 8b where the geometry is close to the ideal case. Nevertheless, it can be seen that close to radii of zero, the sample thickness becomes rather constant. For this case especially the wear of the top of the cone in the anvils' depression is responsible.

The presentation of these extreme cases in Figs. 7 and 8 clearly demonstrates that the hardness and microstructure can be greatly affected for small radii. However, with this explanation, the increasing hardness of US-HPT samples for $r > 6$ mm cannot yet be explained.

Deviations at large radii have been found and discussed before on the basis of arising dead zones at

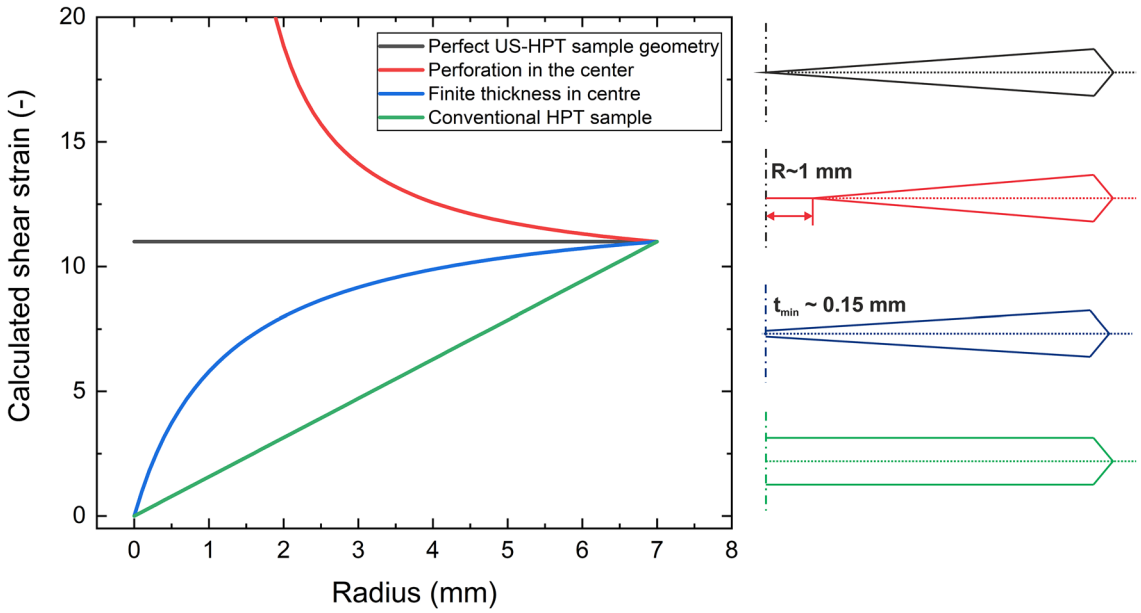

Figure 7 Schematic trend of applied shear strain for US-HPT samples subjected to a rotational angle of 90°. The perfect geometry is compared to samples showing imperfections, either a hole in the center or a remaining finite thickness t_{min} at $r = 0$ mm. For comparison, the linearly increasing applied shear strain for HPT, Eq. (1), for the same degree of rotation is shown as well.

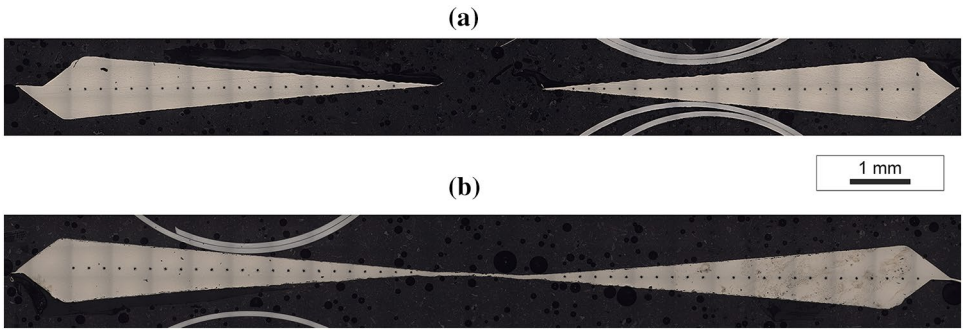

Figure 8 Cross sections of samples using US-HPT. **a** Punctured sample. Due to the large perforation, the sample was not included into the study. **b** Sample with finite nearly constant thickness spanning several millimeters. Scale bar applies for both images.

the edges of the HPT-sample [17–19]. At the transition from the maximum hardness at constant thickness (in this study $r = 7$ mm) to the outer edge where the thickness is steadily decreasing, the friction conditions should abruptly change from full stick to full slippage. This is to promote homogeneous deformation across the thickness of the sample and no deformation at the edge zone, which is however not feasible. As a consequence, an area arises where material is rather inhomogeneously deformed with an extended area of a dead zone and another section towards the middle plane of the sample, which becomes even more deformed than the areas of constant thickness due to the constantly decreasing thickness toward the very edge of the sample. This area can therefore exhibit a further increase of hardness, especially when the applied strain is too low to realize a stagnation of the increase of hardness (saturation).

Both limiting zones at small and large radii that counteract the strain uniformity can be possibly mitigated by technical improvements. To obtain or improve homogeneity at small radii, it is advisable to use anvils and samples being exactly pre-shaped by CNC turning so that large compressive plastic deformations at small radii are avoided. This idea is similar to the one used in this study, where the material was preconditioned by pre-deformation and recrystallization; however, pre-shaping can be applied to all materials classes. In contrast, heat treatments in more complex alloys than pure metals may lead to undesired microstructural changes, for example the formation of undesired phases.

In addition, the use of ultrahigh strength anvils, such as tungsten carbide, helps to avoid plastic deformation and flattening of the center cone (compare Fig. 1b with Fig. 8b) that impacts directly the local sample geometry. For large radii, an adequate polishing of the outer rim of the anvils could contribute to reduce the friction between sample and anvils, which induces an additional deformation. Finally, as the main intention of US-HPT is to synthesize larger volumes of uniform strain, the usage of larger HPT-devices and samples [17] would help to reduce the influence of the center and edge region of the sample and geometry deviations will become negligible.

Summary

In this contribution, an adapted anvil design has been presented with the aim to reduce the inherent strain gradient during high-pressure torsion deformation. The underlying process has been termed uniform strain high-pressure torsion (US-HPT). A feasibility study has shown that the process can be used to process samples with extended regions of uniform strain and hardness.

To overcome some of the problems described above, the next steps will encompass the production of a larger set of anvils enabling the deformation of samples with a diameter of 30 mm. With this approach, the region that may experience an inhomogeneous strain distribution will be substantially decreased in relation to the overall sample size. This will enable the production of larger volumes of material featuring a homogeneous microstructure and mechanical properties.

Acknowledgements

The authors thank Dr. Stanislav Zak for the support with confocal laser scanning microscopy.

Author contributions

The authors contributed equally to the conception, experimental design, carrying out measurements and manuscript composition.

Funding

Open access funding provided by Montanuniversität Leoben. This research did not receive any specific grant from funding agencies in the public, commercial or not-for-profit sectors.

Data availability

The data used to support the findings of this study are available upon reasonable request.

Declarations

Conflict of interest The authors declare that there are no potential conflicts of interest in this work.

Ethical approval Not applicable.

References

[1] Zhilyaev AP, Langdon TG (2008) Using high-pressure torsion for metal processing: fundamentals and applications. Prog Mater Sci 53:893–979. https://doi.org/10.1016/j.pmatsci.2008.03.002

[2] Pippan R, Scheriau S, Taylor A, Hafok M, Hohenwarter A, Bachmaier A (2010) Saturation of fragmentation during severe plastic deformation. Annu Rev Mater Res 40:319–343. https://doi.org/10.1146/annurev-matsci-070909-104445

[3] Han J-K, Li X, Dippenaar R, Liss K-D, Kawasaki M (2018) Microscopic plastic response in a bulk nano-structured TiAl intermetallic compound processed by high-pressure torsion. Mater Sci Eng A 714:84–92. https://doi.org/10.1016/j.msea.2017.12.065

[4] Edalati K, Horita Z (2016) A review on high-pressure torsion (HPT) from 1935 to 1988. Mater Sci Eng A 652:325–352. https://doi.org/10.1016/j.msea.2015.11.074

[5] Stüwe HP (2003) Equivalent strains in severe plastic deformation. Adv Eng Mater 5:291–295. https://doi.org/10.1002/adem.200310085

[6] Hohenwarter A, Pippan R (2023) Influence of processing route on the fracture resistance of equal channel angular pressing deformed iron. Adv Eng Mater 25:2201011. https://doi.org/10.1002/adem.202201011

[7] Weissitsch L, Stückler M, Wurster S, Knoll P, Krenn H, Pippan R, Bachmaier A (2020) Strain induced anisotropic magnetic behaviour and exchange coupling effect in Fe-$SmCo_5$ permanent magnets generated by high pressure torsion. Crystals (Basel). https://doi.org/10.3390/cryst10111026

[8] Estrin Y, Molotnikov A, Davies CHJ, Lapovok R (2008) Strain gradient plasticity modelling of high-pressure torsion. J Mech Phys Solids 56:1186–1202. https://doi.org/10.1016/j.jmps.2007.10.004

[9] Todt J, Keckes J, Winter G, Staron P, Hohenwarter A (2018) Gradient residual strain and stress distributions in a high pressure torsion deformed iron disk revealed by high energy X-ray diffraction. Scr Mater 146:178–181. https://doi.org/10.1016/j.scriptamat.2017.11.037

[10] Erbel S (1979) Mechanical properties and structure of extremely strainhardened copper. Met Technol 6:482–486. https://doi.org/10.1179/030716979803276363

[11] Kapp MW, Renk O, Ghosh P, Leitner T, Yang B, Pippan R (2020) Plastic strain triggers structural instabilities upon cyclic loading in ultrafine-grained nickel. Acta Mater 200:136–147. https://doi.org/10.1016/j.actamat.2020.08.049

[12] Zhilyaev AP, Lee S, Nurislamova GV, Valiev RZ, Langdon TG (2001) Microhardness and microstructural evolution in pure nickel during high-pressure torsion. Scr Mater 44:2753–2758. https://doi.org/10.1016/S1359-6462(01)00955-1

[13] Hafok M, Pippan R (2008) High-pressure torsion applied to nickel single crystals. Phil Mag 88:1857–1877. https://doi.org/10.1080/14786430802337071

[14] Popov VV, Popova EN, Osinnikov EV (2023) Specific features of grain boundaries in nickel processed by high-pressure torsion. Mater Trans 64:1401–1409. https://doi.org/10.2320/matertrans.MT-MF2022012

[15] Edalati K, Horita Z, Langdon TG (2009) The significance of slippage in processing by high-pressure torsion. Scr Mater 60:9–12. https://doi.org/10.1016/j.scriptamat.2008.08.042

[16] Beygelzimer Y, Estrin Y, Davydenko O, Kulagin R (2023) Gripping prospective of non-shear flows under high-pressure torsion. Materials. https://doi.org/10.3390/ma16020823

[17] Hohenwarter A, Pippan R (2019) Sample size and strain-rate-sensitivity effects on the homogeneity of high-pressure torsion deformed disks. Metall Mater Trans A Phys Metall Mater Sci 50:601–608. https://doi.org/10.1007/s11661-018-4989-1

[18] Lee DJ, Yoon EY, Park LJ, Kim HS (2012) The dead metal zone in high-pressure torsion. Scr Mater 67:384–387. https://doi.org/10.1016/j.scriptamat.2012.05.024

[19] Lee DJ, Kim HS (2014) Finite element analysis for the geometry effect on strain inhomogeneity during high-pressure torsion. J Mater Sci 49:6620–6628. https://doi.org/10.1007/s10853-014-8283-3